HHS Public Access

Author manuscript

J Vasc Interv Radiol. Author manuscript; available in PMC 2020 September 01.

Published in final edited form as:

J Vasc Interv Radiol. 2019 September ; 30(9): 1512–1521.e3. doi:10.1016/j.jvir.2018.11.032.

Evaluation of venous stenosis angioplasty in a murine AVF model

Chuanqi Cai, M.D.[1,2], **Binxia Yang, MD, Ph.D.**[2], **Sreenivasulu Kilari, Ph.D.**[2], **Yiqing Li, M.D.**[1], **Chenglei Zhao, M.D.**[2,3], **Amit Sharma, Ph.D.**[2], **Sanjay Misra, M.D.**[2,4,5]

[1]Department of Vascular Surgery, Union Hospital, Tongji Medical College, Huazhong University of Science and Technology, Wuhan, Hubei, China;

[2]Vascular and Interventional Radiology Translational Laboratory, Department of Radiology;

[3]Department of Vascular Surgery, The Second Xiangya Hospital, Central South University, Changsha, Hunan, China

[4]Department of Biochemistry and Molecular Biology Mayo Clinic, Rochester, MN

[5]Department of Radiology, Vascular and Interventional Radiology Mayo Clinic Rochester, MN

Abstract

Purpose: To develop a clinically relevant model of percutaneous transluminal angioplasty (PTA) of venous stenosis in mice with arteriovenous fistula (AVF) and test the hypothesis, that there is increased wall shear stress (WSS) after PTA and histologically characterize the vessels.

Methods: Twenty C57BL/6J male mice, 6–8 weeks old underwent partial nephrectomy to create CKD. Twenty-eight days later, an AVF was created from the right external jugular vein to the left carotid artery. Fourteen days later, an angioplasty or sham procedure was performed and the mice were sacrificed 14 days later for histologic evaluation to identify the cells contributing to the vascular remodeling (α-SMA, FSP-1, CD31, CD68), proliferation (Ki-67), cell death (TUNEL), and hypoxia staining (HIF-1α). Histomorphometric analysis was performed to assess lumen area, neointima area and cellular density. Ultrasound was performed weekly after creation of the AVF.

Results: Venous stenosis occurs 14 days after creation of AVF. PTA treated vessels have significantly higher WSS, average peak systolic velocity, with increased lumen vessel area and decreased neointima + media area than sham controls. There is a significant decrease in the staining of smooth muscle cells, fibroblasts, macrophage, HIF-1α, proliferation and apoptosis and an increase in CD31 (+) cells.

Address correspondence to: Sanjay Misra, MD, FSIR, FAHA Department of Radiology, Professor of Radiology, Mayo Clinic, 200 First St SW, Rochester, MN 55905, Telephone: 507-293-3793, Fax: 507-255-7872, misra.sanjay@mayo.edu.

Disclosures: This work has been funded by NIH grants to SM (HL098967 and DK107870).

Conflict of Interest statement: The results presented in this paper have not been published previously in whole or part, or in abstract format.

Conclusion: A clinically relevant model of PTA of venous stenosis in mice was created. PTA treated vessels have increased lumen vessel area and wall shear stress. The alterations in tissue markers of vascular remodeling, tissue hypoxia, proliferation, and cell death may be implications for future design of drug and device development.

Keywords

angioplasty; arteriovenous fistula; murine model; maturation; venous stenosis

Introduction

In 2015, there were more than 500,000 patients with end-stage renal disease (ESRD) in the United States [1]. Arteriovenous fistula (AVF) is the preferred vascular access for hemodialysis but the primary patency rates of AVF at one year and two years are 60% and 51%, respectively as reported in several studies [2, 3]. Venous stenosis is one of the main reasons for AVF failure [4–6] and this is treated with percutaneous transluminal angioplasty (PTA) [2, 6] but the primary patency rate of PTA at 6, 12, and 24 months is 61%, 42% and 35%, respectively [7].

Histologically, venous neointimal hyperplasia (VNH) is responsible for PTA failure. Unfortunately, there is lack of understanding of the molecular mechanisms responsible for VNH formation. To understand the mechanisms, animal models have been created. Using large animal models, one can test the efficacy of interventional devices however the models have limitations, as often stenosis needs to be induced using a stent or clip and these models often have normal kidney function [8, 9]. A murine model that uses PTA is advantageous because it would allow genetic or pharmacologic manipulation to understand the mechanism responsible for VNH formation [10, 11]. These models are difficult to develop because the size of the mice veins is approximately 1-mm and smaller than the commercially available PTA catheters.

Histologically, VNH is characterized by increased staining of fibroblasts [fibroblast specific protein-1 (FSP-1)], smooth muscle cells [α-smooth muscle cell actin (+), α-SMA], and macrophages (CD68) [10, 12]. Moreover, it is hypothesized that wall shear stress (WSS) and hypoxic injury due to an increase in hypoxia inducible factor-1 alpha (HIF-1α), a transcription factor, are responsible for VNH formation after AVF placement [12–15]. The purpose of the present paper was to develop a clinically relevant model of PTA of venous stenosis in mice and test the hypothesis, that there is increased wall shear stress (WSS) after PTA and histologically characterize the vessels. A better understanding of these mechanisms may help guide the development of new therapeutic interventions for preventing restenosis.

Materials and Methods

Institutional Animal Care and Use committee approval was obtained for this study. Twenty C57BL/J6 male mice (Jackson Laboratories, Bar Harbor, ME) aged 6–8 weeks old were housed at 12/12 h light/dark cycles, 22°C, and 41% relative humidity with access to food and water ad libitum. Mice were anesthetized using a combination of ketamine (120 mg/kg) and xylazine (10 mg/kg) administered using a intraperitoneal injection prior to all

procedures and maintained using ketamine (40 mg/kg) and xylazine (3 mg/kg). Before surgery, one dose of buprenorphine (0.05–0.1 mg/kg body sc) was administered for pain relief. After each surgery, 0.5-mL saline was injected subcutaneously, and the mice were kept on a warm blanket and were monitored.

CKD with AVF procedure

At day 0, chronic kidney disease was created by surgical ligation of the arterial blood supply to the upper pole of left kidney accompanied by removal of the right kidney as described elsewhere [11, 16, 17]. Four weeks later, an arteriovenous fistula was created by anastomosing the end of the right external jugular vein (REJV) to the side of the left common carotid artery (LCCA, Supplementary Fig. 1a). The REJV was isolated using a dissecting microscope (Leica Microsystems M125, Wetzlar, Germany) and the distal end clamped, ligated, and flushed with 1-mL of heparinized saline (100 U/mL). The LCCA was dissected to its bifurcation, and the proximal and distal ends were clamped. An incision of approximately 1 mm in length was made and an end-to-side anastomosis was created using an 11–0 nylon suture (Aros Surgical Instruments Corporation, Newport Beach, CA). The REJV and LCCA were unclamped and the patency of the AVF was evaluated visually by the mixing of the venous and arterial blood.

PTA or sham procedure

Fourteen days after AVF creation, anesthesia was induced and a PTA or sham procedure was performed. The REJV and LCCA were isolated under the dissecting Leica operating microscope and clamped. The REJV was punctured and flushed with 1-mL of heparinized saline (100 U/mL). The balloon catheter (1.2-mm diameter by a 6-mm long angioplasty balloon, Medtronic Sprinter Legend, Minneapolis, MN) was advanced and inflated to 14 ATM (pressure) for 30 seconds (Supplementary Fig. 1c). The balloon was deflated and removed and then the lumen was flushed with 1-mL of heparinized saline (100 U/mL). The puncture site was sutured with 11–0 nylon suture. The REJV and LCCA were unclamped and the patency confirmed visually as described earlier. For sham procedure, the REJV and LCCA were dissected free only. The diameter of the jugular vein was measured intraoperatively.

Doppler Ultrasound (US) examination

A high-frequency 20-MHz transducer probe Doppler scanner (Doppler Flow Velocity System, INDUS Instruments, Houston, TX) was used to evaluate the AVF patency and blood flow velocity. Briefly, anesthesia was induced as described earlier. The mouse was fixed on a warm plate and ECG monitoring performed. All Doppler US procedure was performed by the same operator throughout the study. Eight consecutive cycles were recorded. Murine peak velocity data were analyzed using Doppler signal processing workstation version 1.627 (Doppler Flow Velocity System, INDUS Instruments) utilizing the murine peripheral blood flow mode.

Wall shear stress

The average wall shear stress (WSS) at different time points was calculated by using the velocity and diameter data measured intraoperatively at time of PTA or sham and at sacrifice according to the following equation: $WSS = 4\eta V/r$. Here η is blood viscosity, V is flow velocity (cm/s), and r is the radius (cm). Blood viscosity was assumed to be constant at 0.035 poise [13].

Murine Tissue Collecting and Processing

Fourteen days after both PTA or sham procedure, both jugular vein samples were dissected and prepared for histomorphometric analysis by fixing them in 10% formalin reagent (Fisher Scientific, Pittsburgh, PA). Each jugular vein was embedded in paraffin lengthwise as described previously [11, 13, 18]. Typically, an average of 40 to 60 consecutive 4-μm sections were obtained per jugular vein per animal for analysis.

Immunohistochemistry (online supplemental appendix)

Immunohistochemistry was performed on paraffin-embedded sections from the PTA treated vessels or sham control vessels to evaluate cellular changes using the EnVision (Dako, Carpinteria, CA) method with a heat-induced antigen-retrieval step [11]. The following primary antibodies were used: CD31 (ab28364–100; 1:200; Abcam, Cambridge, UK), CD68 (ab125212; 1:1000; Abcam), α-SMA (ab5694; 1:800; Abcam), Ki-67 (ab9260; 1:350; Abcam), FSP-1 (07–2274, 1:1000; EMD Millipore, USA), and HIF-1α (NB100–105; 1:1000; Novus Biologicals, St. Louis, MO). Negative controls had staining performed with the primary antibody omitted. The secondary antibody used was either Envision HRP labeled polymer anti-rabbit or anti-mouse (Dako, Carpinteria, CA).

TUNEL staining (online supplemental appendix)

TUNEL assay was performed on paraffin-embedded sections from the PTA treated and sham controls to evaluate apoptosis according to the manufacturer's instructions (TACS® 2 TdT DAB in situ Apoptosis Detection Kit, Thermo Fisher Scientific, Gaithersburg, MD) [11, 19]. Stained slides without TdT Enzyme were used as negative control.

Picrosirius red and Verhoeff-Van Gieson staining (VVG) staining (online supplemental appendix)

Picrosirius red staining was performed on the PTA treated or sham control veins collected to evaluate collagen 1 and 3 as described previously [11]. Verhoeff-Van Gieson staining (VVG) was performed to examine elastic fibers on the PTA treated and sham treated outflow veins according to the manufacturer's directions (Newcomer Supply, Inc, Middleton, WI).

Picrosirius red and Verhoeff-Van Gieson staining (VVG) staining (online supplemental appendix)

PTA treated vessels and sham controls were stained for Hematoxylin and eosin (H and E) to assess venous remodeling and next viewed using a Zeiss Imager. Images were digitized to capture a minimum of 1936 × 1460 pixels covering one entire cross-section from each vessel that had been treated with PTA or sham utilizing M2 Microscope (Carl Zeiss) with an

Axiocam 503 color camera (Carl Zeiss) and analyzed using ZEN 2 blue edition version 2.0 (Carl Zeiss). The H and E were highlighted, in turn, by selecting the appropriate red-green-blue color intensity range and then counted as described elsewhere [10].

Statistical Analysis

Results are expressed as mean ± standard error of the mean (SEM). Statistical differences were tested by either a one way or two way analysis of variance (ANOVA) followed by a post hoc Bonferroni's correction. The level of significance was set at $^{*}P<0.05$, $^{**}P<0.001$, or $^{\#}P<0.0001$. GraphPad Prism version 7 (GraphPad Software Inc, La Jolla, CA) was used for all statistical analyses.

Results

Surgical outcomes:

Six mice died after multiple surgeries and one mouse was excluded due to a small REJV and thickened LCCA. The study consisted of 13 animals divided into the PTA treated mice (N=6) and sham mice (N=7).

Changes in diameter, lumen vessel area, and area of neointima + media

The sequential changes in the diameter of the jugular vein were determined by intraoperative measurement after AVF placement, during the PTA or sham procedures, and at sacrifice (Fig. 1a). In the sham group, the average diameter of the jugular vein at day 42 was significantly larger than day 28 (Day 42: 1.05 ± 0.07 mm, Day 28: 0.71 ± 0.04 mm, average increase: 148%, P<0.01) but by day 56, it was significantly smaller than day 42 (Day 56: 0.71 ± 0.11 mm, Day 42: 1.05 ± 0.07 mm, average reduction: 32%, P<0.05). In the PTA group, there was a significant increase in the average diameter of jugular vein of the day 42 group compared to the day 28 (Day 42: 1.02 ± 0.02 mm, Day 28: 0.72 ± 0.04 mm, average increase: 142%, P<0.01) and it remained significantly higher in the day 56 group compared to day 28 (Day 56: 1.07 ± 0.08 mm, Day 28: 0.72 ± 0.04 mm, average increase: 149%, P<0.01).

A representative Hematoxylin and eosin stained jugular vein from PTA and sham groups is shown (Fig. 1b). The average lumen vessel area from the PTA group was significantly higher than the sham control (PTA: 68327.69 ± 4572.71 μm^2, sham: 35396.68 ± 9645.51 μm^2, average increase: 193%, P<0.01, Fig. 1c). In the sham group, Verhoeff-Van Gieson (VVG) staining demonstrated an intact internal elastic layer (IEL) while in PTA vessels, the IEL was disrupted (Fig. 1d). The average cell density in the neointima and media was significantly reduced as well (PTA: 9742.95 ± 627.49/mm^2, sham: 13552.87 ± 1325.92/mm^2, average decrease: 28%, P<0.05, Fig. 1e). The average area of the neointima and media was significantly decreased in the PTA group when compared to the sham group (PTA: 135706.90 ± 33778.38 μm^2, sham: 295280.30 ± 18425.44 μm^2, average decrease: 54%, P<0.001, Fig. 1f).

Peak velocity and wall shear stress

The peak velocity (PV) in cm/s of the jugular vein was determined from the Doppler ultrasound assessment at day 35, 42, 49 and 56 (sham: n=6, PTA: n=5, Fig. 2a). There was a significant decrease in the average PV in the sham group compared to the PTA group at day 56 (sham: 51.11 ± 20.39 cm/s, PTA: 159.16 ± 25.57 cm/s, average decrease: 68%, P<0.05, Fig. 2b). In the sham group, there was a significant decrease in the average PV at day 56 compared to day 35 (Day 56: 51.11 ± 20.39 cm/s, Day 35: 143.87 ± 16.78 cm/s, average decrease: 64%, P<0.01), day 56 vs. day 42 (Day 56: 51.11 ± 20.39 cm/s, Day 42: 163.38 ± 9.19 cm/s, average decrease: 69%, P<0.001), and day 56 vs. day 49 (Day 56: 51.11 ± 20.39 cm/s, Day 49: 118.13 ± 25.21 cm/s, average decrease: 57%, P<0.05). In the PTA group, there was no difference at any of the time points when compared to each other.

Wall shear stress has not been systematically investigated after PTA of venous stenosis in AVFs [12–15]. By day 56, the average WSS was significantly higher in PTA group when compared to sham group (PTA: 413.20 ± 56.98 dyne/cm^2, sham: 178.18 ± 64.87 dyne/cm^2, average increase: 232%, P<0.05, Fig. 2c).

Immunostaining of α-SMA, Fsp-1, CD68, and CD31

Immunostaining for Fsp-1 α-SMA, and CD68 at the jugular vein were performed. α-SMA (+) cells were localized to the neointima in the sham vessels. In PTA vessels, they were located throughout the vessel wall (Fig. 3a). Semiquantitative analysis demonstrated that there was a significant decrease in the average α-SMA index of PTA vessels compared to sham controls (PTA: 9.38 ± 2.09%, sham: 21.89 ± 1.94%, average decrease: 57%, P<0.01, Fig. 3c). Fsp-1 (+) cells were localized to the neointima in the sham control vessels where as in PTA vessels; they were located throughout the vessel wall (Fig. 3b). There was a significant decrease in the average Fsp-1 index in the PTA vessels compared to sham controls (PTA: 5.57 ± 0.56%, sham: 14.80 ± 1.47%, average decrease: 62%, P<0.01, Fig. 3d). Next, the expression of CD31 staining was performed to determine if reendotheiliazition occurred after PTA. This demonstrated that there were CD31 (+) cells forming microvessels that were localized to the adventitia and media of PTA treated vessels compared to control shams (Fig. 4a). In contrast, in sham controls, the CD31 (+) cells were found lining the endothelium, which was denuded, whereas, in the PTA treated vessels, the endothelium was intact with continuous CD31 (+) cells. The average CD31 index of PTA vessels was significantly increased compared to sham controls (PTA: 7.94 ± 1.19%, sham: 2.88 ± 0.64%, average increase: 276%, P<0.01, Fig. 4c). CD68 (+) cells were seen in the neointima and subendotheilial space. In the PTA vessels, it was localized to the media and adventitia (Fig. 4b). There was a significant reduction in the average CD68 index in PTA vessels compared to sham control vessels (PTA: 5.68 ± 1.81%, sham: 13.73 ± 1.82%, average decrease: 59%, P<0.05, Fig. 4d).

Collagen staining

Sirius red staining (Supplementary Fig. 2a) was performed in PTA vessels compared to sham controls. The average intensity of Sirius red staining in the PTA vessels was significantly increased compared to sham controls (PTA: 26.82 ± 4.22%, sham: 19.44 ± 3.88%, average increase: 138%, P<0.01, Supplementary Fig. 2b).

Cellular proliferation and TUNEL staining

Cellular proliferation (Fig. 5a) was performed in PTA vessels compared to sham control vessels. In sham controls, there was an increase in Ki-67 (+) cells located in the neointima and media. In PTA vessels, Ki-67 (+) cells were decreased and scattered in the neointima and adventitia. The average Ki-67 index in PTA vessels was significantly reduced when compared to sham controls (PTA: 3.92% ± 0.71%, sham: 11.03% ± 0.57%, average decrease: 64%, $P<0.001$, Fig. 5c). TUNEL staining (Fig. 5b) was performed in PTA vessels compared to sham control vessels. In sham controls, the majority of TUNEL (+) cells were found in the neointima and media. In PTA vessels, TUNEL (+) cells were found scattered throughout the adventitia. There was a significant decrease in the average TUNEL index in the PTA vessels compared to sham controls (PTA: 1.65% ± 0.25%, sham: 4.70% ± 0.74%, average decrease: 65%, $P<0.01$, Fig. 5d).

Hif-1α staining

Hif-1α staining (Supplementary Fig. 3a) was performed in PTA vessels compared to sham control vessels. There was a significant decrease in the average Hif-1α index in the PTA vessels compared to sham controls (PTA: 4.66% ± 0.81%, Sham: 9.91% ± 0.92%, average decrease: 53%, $P<0.01$, Supplementary Fig. 3b).

Discussion

In the present study, a new murine model of PTA of venous stenosis was created in mice with chronic kidney disease and an arteriovenous fistula. A venous stenosis was allowed to develop that was treated with angioplasty thus simulating the clinical scenario. The histomorphometric, shear stress, and hemodynamic changes in both PTA and sham vessels were assessed. Using this model, in PTA compared to sham controls, there was a disruption of the IEL leading to reendothelialization by CD31 (+) cells. Moreover, there was a significant reduction in cellular proliferation and TUNEL with a decrease in FSP-1, α-SMA, CD68, and HIF-1α staining. In PTA vessels compared to controls, there is a significant increase in lumen vessel area, decrease in area of the neointima plus media, decrease in cell density, and increase in collagen staining. Hemodynamically, there is a significant increase in the peak velocity and average WSS in PTA vessels when compared to shams.

AVFs have been placed in different animals to investigate the pathophysiological pathways of VNH. The strength of a large animal model is that they can be used for testing interventional devices however the models have limitations as often a stenosis needs to be induced using a stent or clip and these models often have normal kidney function [8, 9]. Murine models are attractive because they have established transgenic animals that can be utilized to unveil the molecular mechanism of stenosis formation [10]. When compared with other published murine AVF models, this model was the most similar with the clinical scenario for several reasons including the mice had CKD and a venous stenosis had formed before it was treated with PTA. To date, there has been no such animal models created. The strength of the current model is that it consists of CKD and oxidative stress with venous stenosis formation treated with PTA [20]. Moreover, other treatments could be evaluated including cutting balloons, drug-coated balloons, drug-eluting stents, and absorbable stents.

In the present study, it was observed that PTA decreased smooth muscle density along with CD68 (+) cells while increasing reendotheiliazition via CD31 (+) cells and disruption of the IEL. This is consistent with angioplasty models of the artery in which there was damage to the IEL, which is accompanied with CD31 (+) cells infiltration which allows healing to occur [21]. This has clinical implications for design of drug-coated balloons for reducing stenosis formation in stenotic AVF [22]. It would be very important to have technologies designed that would allow CD31 repopulation to occur as medications such as metformin can inhibit reendotheiliazition after experimental placement of DES [23, 24].

Moreover, in PTA treated vessels, there was a reduction in proliferation and TUNEL staining. The decrease in proliferation is consistent with other treatments aimed at primary prevention of stenosis formation at the time of AVF creation in experimental murine models. This has been found to be associated with increase in lumen vessel area; however, there was an increase in TUNEL staining [11, 19, 25]. Finally PTA vessels had an increase in the expression of collagen as assessed with Sirius red staining. This observation has implications for using cutting balloons and high-pressure balloons, which have been shown to be superior for treating stenotic AVF that were resistant to PTA, which may be biologically caused by the increased expression of collagen [26].

Finally, PTA vessels had a significant decrease in the average area of the neointima plus media accompanied with an increase in lumen vessel area when compared to sham vessels. This finding is consistent with clinical outcomes of PTA which demonstrate a decrease in stenosis associated with AVF and other vascular stenosis [22]. In addition, there was a decrease in HIF-1α in PTA vessels. This is different than what has been observed in stenotic outflow veins removed from AVF. The implication is that the biology of stenosis formation in PTA vessels maybe different than stenosis associated with AVF placement [16] or polytetrafluoroethylene bypass grafts used in the arterial system [27–30].

Published societal guidelines recommend ultrasound evaluation as a diagnostic tool to detect malfunctioning AVFs in patients with clinical signs or symptoms of AVF dysfunction [31, 32]. In the present study, Doppler US was performed in each mouse to determine the peak velocity (PV). In the sham controls, the mean PV decreased until the animals were sacrificed. However, in the PTA group, the mean PV increased and remained significantly higher than the sham group. In addition, the mean wall shear stress and lumen vessel area were significantly increased in PTA vessels compared to sham controls. This is different than what has been observed in experimental animal models with arteriovenous polytetrafluoroethylene grafts in which there is an increase in WSS with the formation of a venous stenosis [13–15].

There are some limitations to the present study. One weakness is that the vessels utilized were smaller than what is seen clinically and the common carotid artery is a low resistance vessel compared to the extremity vessels, which are high resistance. Because of the diameter of the inflow artery, the PTA procedure was mostly performed in outflow vein; hence, PTA treatment failed to treat the inflow artery. Inflow arterial stenosis is uncommon in a newly created AVF [33]. In the future, animals will be followed for a longer period of time to observe the late changes that occur in vessels treated with PTA.

In summary, a clinically relevant model of PTA of venous stenosis associated with hemodialysis AVF was created in mice with CKD. Using this model, it was 0bserved that there is increase in lumen vessel area and shear stress with a decrease in α-SMA, FSP-1, CD68, HIF-1α, proliferation, and cell death with an increase in CD31 in PTA vessels. In the future, this model could be used to understand the mechanism of PTA failure that occurs in patients with hemodialysis AVF.

Supplementary Material

Refer to Web version on PubMed Central for supplementary material.

References:

1. Saran R, et al., US Renal Data System 2017 Annual Data Report: Epidemiology of Kidney Disease in the United States. American Journal of Kidney Diseases, 2018 71(3, Supplement 1): p. A7. [PubMed: 29477157]
2. Clinical practice guidelines for vascular access. Am J Kidney Dis, 2006 48 Suppl 1: p. S176–247. [PubMed: 16813989]
3. Al-Jaishi AA, et al., Patency rates of the arteriovenous fistula for hemodialysis: a systematic review and meta-analysis. Am J Kidney Dis, 2014 63(3): p. 464–78. [PubMed: 24183112]
4. Dhingra RK, et al., Type of vascular access and mortality in U.S. hemodialysis patients. Kidney Int, 2001 60(4): p. 1443–51. [PubMed: 11576358]
5. Riella MC and Roy-Chaudhury P, Vascular access in haemodialysis: strengthening the Achilles' heel. Nat Rev Nephrol, 2013 9(6): p. 348–57. [PubMed: 23591442]
6. Tonelli M, et al., Access flow monitoring of patients with native vessel arteriovenous fistulae and previous angioplasty. J Am Soc Nephrol, 2002 13(12): p. 2969–73. [PubMed: 12444216]
7. Bountouris I, et al., Is Repeat PTA of a Failing Hemodialysis Fistula Durable? Int J Vasc Med, 2014 2014: p. 369687. [PubMed: 24587906]
8. Trerotola SO, et al., Comparison of Gianturco Z stents and Wallstents in a hemodialysis access graft animal model. J Vasc Interv Radiol, 1995 6(3): p. 387–96. [PubMed: 7647440]
9. Varcoe RL, et al., An arteriovenous fistula model of intimal hyperplasia for evaluation of a nitinol U-Clip anastomosis. Eur J Vasc Endovasc Surg, 2012 43(2): p. 224–31. [PubMed: 22104322]
10. Brahmbhatt A, et al., The role of Iex-1 in the pathogenesis of venous neointimal hyperplasia associated with hemodialysis arteriovenous fistula. PLoS One, 2014 9(7): p. e102542. [PubMed: 25036043]
11. Yang B, et al., Adventitial transduction of lentivirus-shRNA-VEGF-A in arteriovenous fistula reduces venous stenosis formation. Kidney Int, 2014 85(2): p. 289–306. [PubMed: 23924957]
12. Brahmbhatt A, et al., The molecular mechanisms of hemodialysis vascular access failure. Kidney Int, 2016 89(2): p. 303–316. [PubMed: 26806833]
13. Misra S, et al., Evolution of shear stress, protein expression, and vessel area in an animal model of arterial dilatation in hemodialysis grafts. J Vasc Interv Radiol, 2010 21(1): p. 108–15. [PubMed: 20123196]
14. Misra S, et al., Assessment of Wall Shear Stress Changes in Arteries and Veins of Arteriovenous Polytetrafluoroethylene Grafts Using Magnetic Resonance Imaging. Cardiovasc Intervent Radiol, 2006 29: p. 624–629. [PubMed: 16729233]
15. Misra S, et al., Increased shear stress with upregulation of VEGF-A and its receptors and MMP-2, MMP-9, and TIMP-1 in venous stenosis of hemodialysis grafts. Am J Physiol Heart Circ Physiol, 2008 294(5): p. H2219–30. [PubMed: 18326810]
16. Misra S, et al., Increased expression of hypoxia-inducible factor-1 alpha in venous stenosis of arteriovenous polytetrafluoroethylene grafts in a chronic renal insufficiency porcine model. J Vasc Interv Radiol, 2008 19(2 Pt 1): p. 260–5. [PubMed: 18341959]

17. Janardhanan R, et al., The Role of Repeat Administration of Adventitial Delivery of Lentivirus-shRNA-Vegf-A in Arteriovenous Fistula to Prevent Venous Stenosis Formation. J Vasc Interv Radiol, 2016 27(4): p. 576–83. [PubMed: 26948326]
18. Yang B, et al., The mouse arteriovenous fistula model. J Vasc Interv Radiol, 2009 20(7): p. 946–50. [PubMed: 19555889]
19. Janardhanan R, et al., Simvastatin reduces venous stenosis formation in a murine hemodialysis vascular access model. Kidney Int, 2013 Aug(84(2)): p. 338–52.
20. Simon DI, et al., Decreased neointimal formation in Mac-1(−/−) mice reveals a role for inflammation in vascular repair after angioplasty. J Clin Invest, 2000 105(3): p. 293–300. [PubMed: 10675355]
21. Bauters C and Isner JM, The biology of restenosis. Prog Cardiovasc Dis, 1997 40(2): p. 107–16. [PubMed: 9327827]
22. Trerotola SO, et al., Drug Coated Balloon Angioplasty in Failing AV Fistulas: A Randomized Controlled Trial. Clin J Am Soc Nephrol, 2018 13(8): p. 1215–1224. [PubMed: 30042225]
23. Habib A, et al., Metformin impairs vascular endothelial recovery after stent placement in the setting of locally eluted mammalian target of rapamycin inhibitors via S6 kinase-dependent inhibition of cell proliferation. J Am Coll Cardiol, 2013 61(9): p. 971–80. [PubMed: 23449430]
24. Habib A, et al., Metformin impairs endothelialization after placement of newer generation drug eluting stents. Atherosclerosis, 2013 229(2): p. 385–7. [PubMed: 23880192]
25. Yang B, et al., Tracking and Therapeutic Value of Human Adipose Tissue-derived Mesenchymal Stem Cell Transplantation in Reducing Venous Neointimal Hyperplasia Associated with Arteriovenous Fistula. Radiology, 2016 279(2): p. 513–22. [PubMed: 26583911]
26. Aftab SA, et al., Randomized clinical trial of cutting balloon angioplasty versus high-pressure balloon angioplasty in hemodialysis arteriovenous fistula stenoses resistant to conventional balloon angioplasty. J Vasc Interv Radiol, 2014 25(2): p. 190–8. [PubMed: 24315548]
27. Chanakira A, et al., Hypoxia differentially regulates arterial and venous smooth muscle cell proliferation via PDGFR-beta and VEGFR-2 expression. Am J Physiol Heart Circ Physiol, 2012 302(5): p. H1173–84. [PubMed: 22159994]
28. Chanakira A, et al., Hypoxia Differentially Regulates Arterial and Venous Smooth Muscle Cell Migration. PLoS One, 2015 10(9): p. e0138587. [PubMed: 26381529]
29. Lee ES, et al., Association of artery wall hypoxia and cellular proliferation at a vascular anastomosis. J Surg Res, 2000 91(1): p. 32–7. [PubMed: 10816346]
30. Wan J, et al., Supplemental oxygen reverses hypoxia-induced smooth muscle cell proliferation by modulating HIF-alpha and VEGF levels in a rabbit arteriovenous fistula model. Ann Vasc Surg, 2014 28(3): p. 725–36. [PubMed: 24345704]
31. Sidawy AN, et al., The Society for Vascular Surgery: clinical practice guidelines for the surgical placement and maintenance of arteriovenous hemodialysis access. J Vasc Surg, 2008 48(5 Suppl): p. 2s–25s. [PubMed: 19000589]
32. Gornik HL, et al., ACCF/ACR/AIUM/ASE/IAC/SCAI/SCVS/SIR/SVM/SVS/SVU 2013 appropriate use criteria for peripheral vascular ultrasound and physiological testing part II: testing for venous disease and evaluation of hemodialysis access: a report of the american college of cardiology foundation appropriate use criteria task force. J Am Coll Cardiol, 2013 62(7): p. 649–65. [PubMed: 23876422]
33. Rajan DK, et al., Dysfunctional autogenous hemodialysis fistulas: outcomes after angioplasty--are there clinical predictors of patency? Radiology, 2004 232(2): p. 508–15. [PubMed: 15286321]

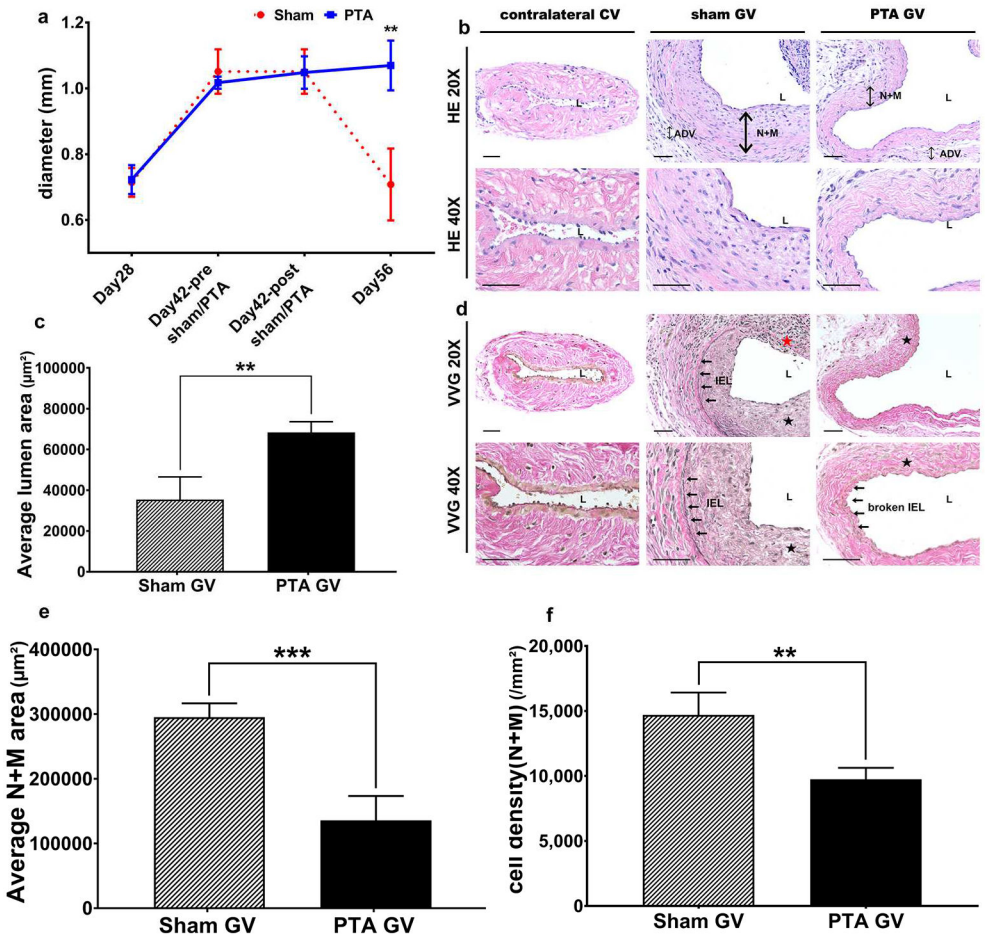

Figure 1: Diameter, lumen vessel area, and area of the neointima + media

(a) By day 56, there is a significant increase in the average intraoperative diameter of the graft veins treated with PTA compared to sham controls (**P<0.01). **B upper row** are representative sections at 20X magnification and **b lower row** is at 40X magnification after Hematoxylin and eosin staining of the contralateral jugular control vein (contralateral CV), sham jugular graft vein (sham GV), and PTA treated jugular graft vein (PTA GV). **(c)** There is a significant increase in the average lumen vessel area of the PTA vessels compared to sham vessels (P<0.01). **D upper row** are representative sections at 20X magnification and **d lower row** is at 40X magnification after Verhoeff-van Gieson staining of the contralateral CV, sham GV, and PTA GV. For CV, there is no internal elastic lamina (IEL). In contrast, the IEL is intact in the sham GV. In the PTA GV, the IEL is broken. **(e)** There is a significant decrease in the average cell density of the neointima + media of the PTA vessels compared with sham vessels (**P<0.01). **(f)** There is a significant decrease in the average area of the neointima + media of the PTA vessels compared with sham vessels (***P<0.001). Each bar represents mean ± SEM of 6–7 animals. ADV, adventitia; L, lumen; N + M, neointima + media; IEL, internal elastic lamina; solid arrows, indicate the IEL; solid black star, neointima; solid red star indicates severe neointimal hyperplasia with loss of IEL. Scale bar is 50-μm.

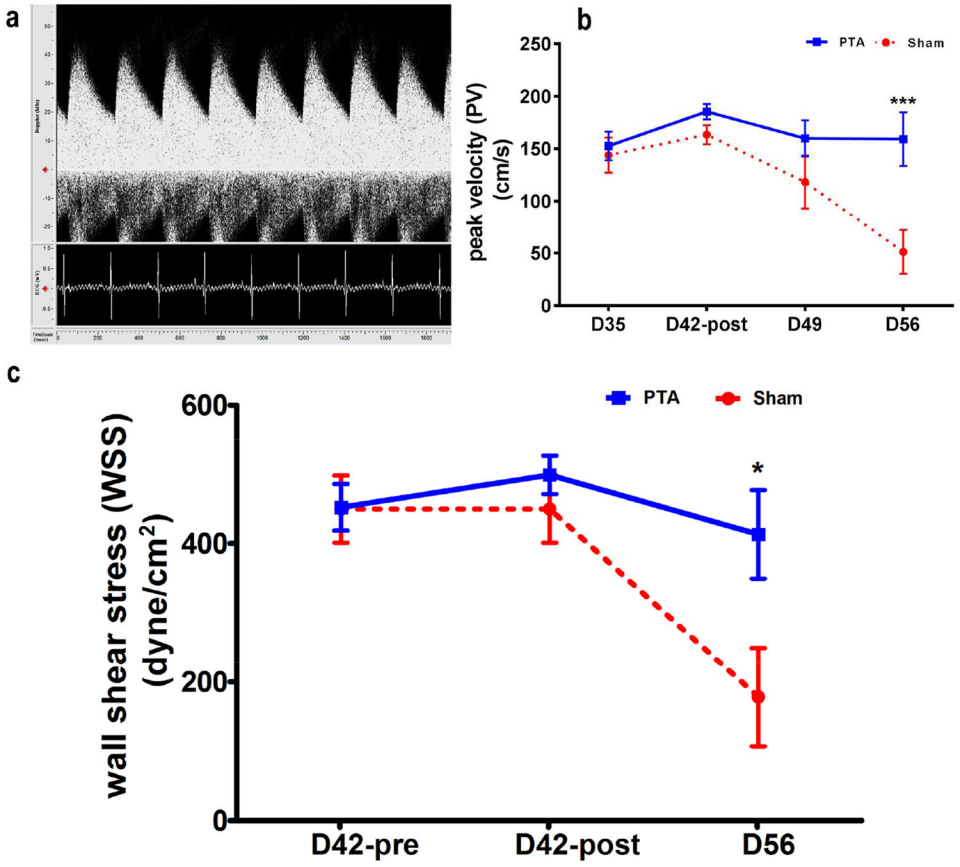

Figure 2: Peak velocity (PV) and wall shear stress (WSS)

A is representative image of the Doppler signal from the jugular graft vein is shown with arterial and spectral broadening waveform. **(b)** By day 56, there is a significant increase in the average peak velocity (PV, ***P<0.001) and **(c)** WSS of the PTA vessels compared with sham vessels (*P<0.05).

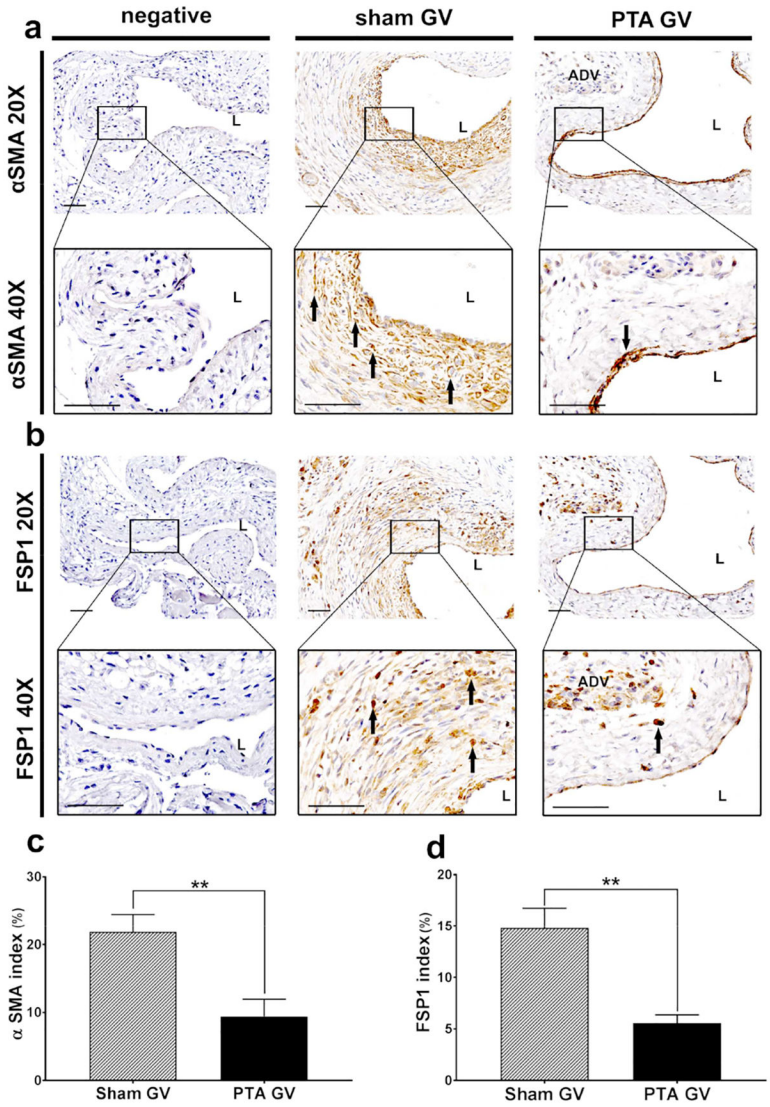

Figure 3: Immunohistochemical staining for α-SMA and FSP-1

A upper row is representative sections at 20X magnification and **b lower row** is at 40X magnification after α-SMA staining of the negative control (negative), sham jugular graft vein (sham GV), and PTA treated jugular graft vein (PTA GV). Qualitatively, there is reduced α-SMA staining in the PTA GV compared to the sham. **B upper row** are representative sections at 20X magnification and **b lower row** is at 40X magnification after FSP-1 staining of the negative, sham GV, and PTA GV. Qualitatively, there is reduced FSP-1 staining in the PTA GV compared to the sham. **(c)** There is a significant reduction in the α-SMA index of the PTA GV compared to sham controls (**P<0.01). **(d)** There is a significant reduction in the FSP-1 index in the PTA GV compared to sham controls (**P<0.01). Each bar represents mean ± SEM of 6–7 animals. ADV, adventitia; L, lumen. Scale bar is 50-μm.

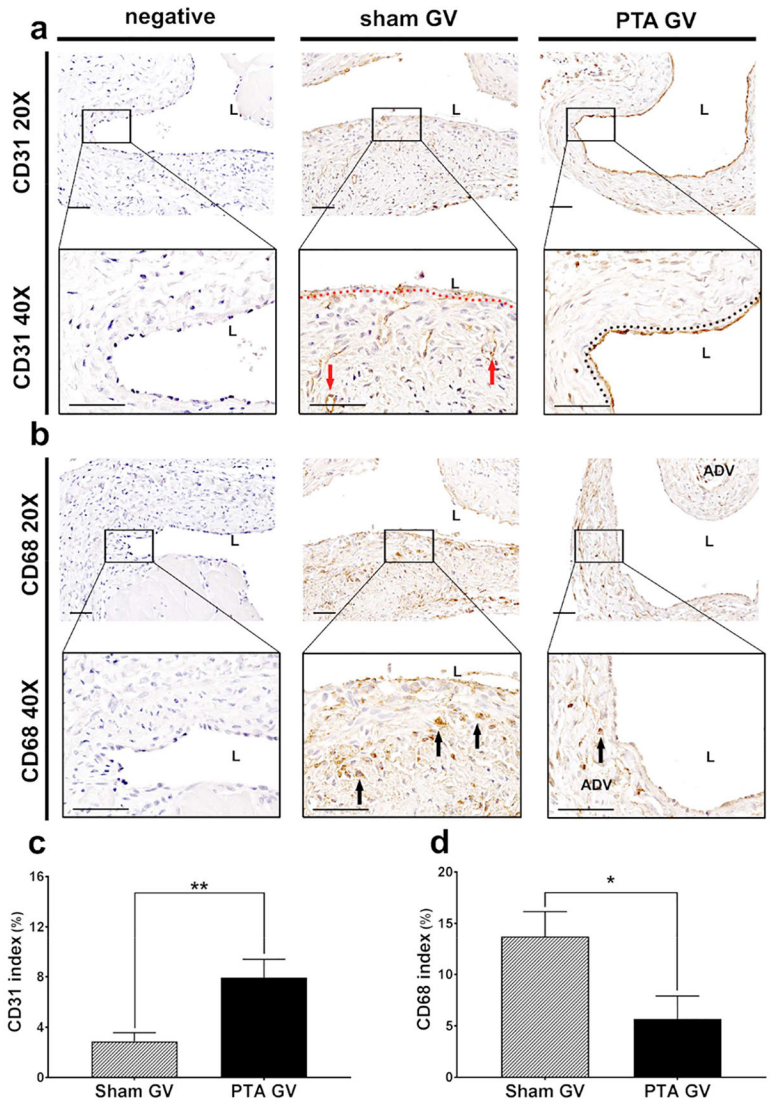

Figure 4: Immunohistochemical staining for CD31 and CD68

A upper row is representative sections at 20X magnification and **a lower row** is at 40X magnification after CD31 staining of the negative control (negative), sham jugular graft vein (sham GV), and PTA treated jugular graft vein (PTA GV). CD31 (+) cells are localized to adventitia and media forming microvessels (red arrow) in PTA treated vessels compared to control shams. In contrast, in sham controls, the CD31 (+) cells staining the endothelium are denuded, whereas, in the PTA treated vessels (single red line), the endothelium is intact with continuous CD31 (+) cells (double black dashed lines). **B upper** row are representative sections at 20X magnification and **b lower row** is at 40X magnification after CD68 staining of the negative control, sham GV, and PTA GV. In sham vessels, CD68 (+) cells are seen in the neointima and subendotheilial space (black arrows). In the PTA vessels, they are localized to the media and adventitia (black arrows). **(c)** There is a significant increase in the CD31 index of the PTA GV compared to sham controls (**P<0.01). **(d)** There is a significant decrease in the CD68 index of the PTA GV compared to sham controls

(*P<0.05). Each bar represents mean ± SEM of 6–7 animals. ADV, adventitia; L, lumen. Scale bar is 50-μm.

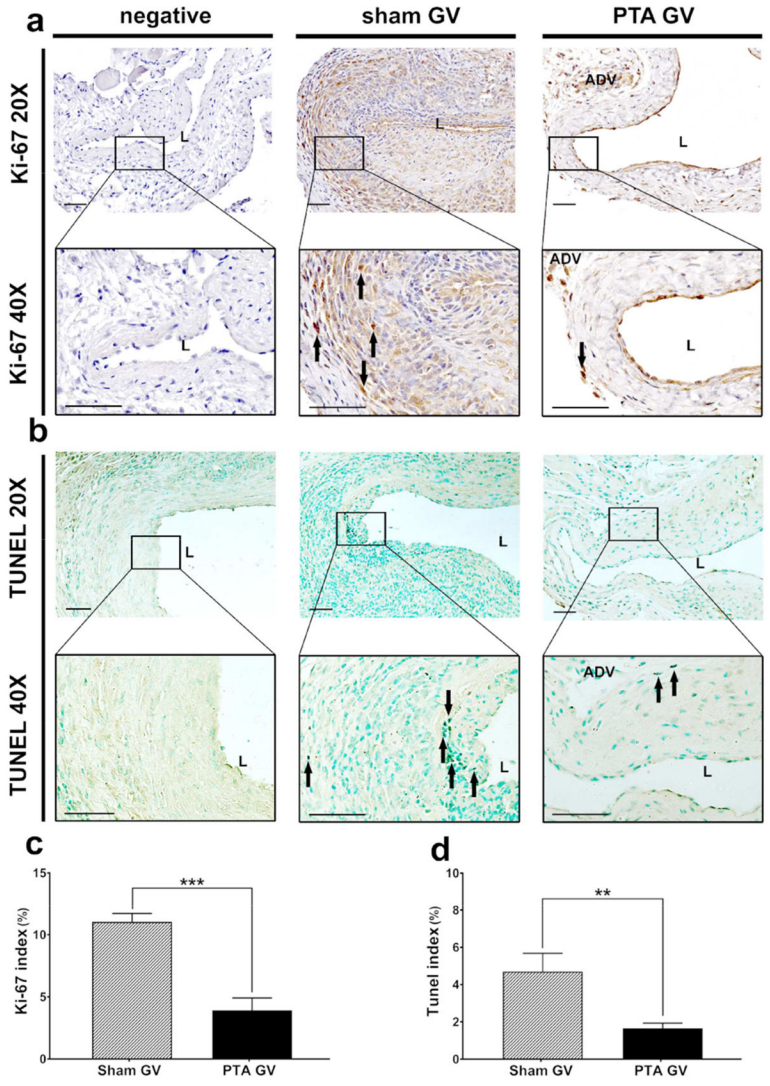

Figure 5: Cellular proliferation and TUNEL staining

A upper row is representative sections at 20X magnification and **a lower row** is at 40X magnification after Ki-67 staining of the negative control (negative), sham jugular graft vein (sham GV), and PTA treated jugular graft vein (PTA GV). Ki-67 (+) cells are localized to neointima and media (black arrows) in sham treated vessels compared to PTA treated shams. **B upper row** are representative sections at 20X magnification and **b lower row** is at 40X magnification after TUNEL staining of the negative control, sham GV, and PTA GV. TUNEL (+) cells are localized to neointima and media (black arrows) in sham vessels compared to PTA GV. **(c)** There is a significant decrease in the mean Ki-67 index of the PTA GV compared to sham controls (***P<0.001). **(d)** There is a significant decrease in the mean TUNEL index of the PTA GV compared to sham controls (**P<0.01). Each bar represents mean ± SEM of 6–7 animals. ADV, adventitia; L, lumen. Scale bar is 50-μm.